

Influence of localization on the carrier diffusion in GaAs/(Al,Ga)As and (In,Ga)(As,N)/GaAs quantum wells: A comparative study

U. Jahn,* S. Dhar, R. Hey, and O. Brandt

Paul-Drude-Institut für Festkörperelektronik, Hausvogteiplatz 5-7, 10117 Berlin, Germany

J. Miguel-Sánchez and A. Guzmán

ISOM, Universidad Politécnica de Madrid, ETSI Telecomunicación, Ciudad Universitaria s/n, 28040 Madrid, Spain

(Received 15 November 2005; revised manuscript received 18 January 2006; published 6 March 2006)

Using a spatially resolved cathodoluminescence technique, we measure the detection-energy and temperature dependence of the diffusion length of excited carriers in GaAs/(Al,Ga)As and (In,Ga)(As,N)/GaAs single quantum wells (QWs), for which the sources of disorder are expected to be entirely different. While in GaAs QWs the interface roughness is a possible source of disorder, in (In,Ga)(As,N) QWs the compositional inhomogeneities are expected to be the prime cause of band structure fluctuations. Thus, the density of the disorder is expected to be even larger in (In,Ga)(As,N)/GaAs QWs as compared to the one in GaAs/(Al,Ga)As QWs. We found that the detection energy as well as temperature dependence of the diffusion length in the two systems are distinctly different. The experimental results are explained in terms of a thermally activated transport in GaAs/(Al,Ga)As QWs and a tunneling-assisted transport in (In,Ga)(As,N)/GaAs QWs. The detection-energy and temperature dependence of the diffusion length can be a powerful tool to distinguish between these two transport mechanisms. Moreover, we have developed a simple theoretical model in order to obtain a better understanding of the diffusion process in (In,Ga)(As,N)/GaAs QWs.

DOI: [10.1103/PhysRevB.73.125303](https://doi.org/10.1103/PhysRevB.73.125303)

PACS number(s): 78.67.De, 73.63.Hs, 78.55.Cr, 78.60.Hk

I. INTRODUCTION

In semiconductor physics, disorder plays an important role in determining the transport properties of a material. There are different sources of disorder in semiconductors and semiconductor-based heterostructures. For example, interface roughness is a potential source of disorder in semiconductor quantum wells (QWs) and superlattices. In semiconductor alloys, the composition is often found to be spatially inhomogeneous, which may result in a large density of fluctuations in the energy band structure. The influence of compositional fluctuations on the band structure of quaternary semiconductor alloys such as (In,Ga)(As,N) is expected to be even stronger than the one in ternary alloys such as (Al,Ga)As and (In,Ga)As. It is found that in (In,Ga)(As,N), which is emerging as a promising material for optical devices operable in the telecommunication wavelength range of 1.3–1.5 μm , nitrogen has a strong influence on the band structure.¹ A significant shrinkage of the band gap has been observed in this material even for N concentrations less than 2%. Moreover, the distribution of N-centered N-Ga_mIn_{4-m} tetrahedra in (In,Ga)(As,N) leads to a large density of band structure fluctuations.² In order to understand the influence of disorder on the transport mechanism, (In,Ga)(As,N) is thus an interesting material to investigate. Transport properties of semiconductor structures are mostly studied by electrical techniques. However, the diffusion of excited carriers can also be investigated by optical methods. Spatially resolved excitation of carriers and the subsequent measurement of the cathodoluminescence (CL) signal in a scanning electron microscope (SEM) is often used to study diffusion mechanisms in semiconductor structures.^{3,4} Time-of-flight measurements⁵ and transient grating experiments⁶ in conjunction with time-

resolved photoluminescence (PL) are among the optical methods applied for the measurement of the carrier diffusivity. The optical methods offer the opportunity to perform an energy selective study of the diffusion processes, which is an advantage over the electrical techniques.

In this work, we have performed a comparative study of the carrier diffusion in GaAs/(Al,Ga)As and (In,Ga)(As,N)/GaAs QWs, where the sources of disorder are expected to be entirely different. While in GaAs/(Al,Ga)As QW structures band structure fluctuations are expected to be caused by interface roughness, compositional fluctuations are probably the prime cause of disorder in (In,Ga)(As,N)/GaAs QWs. Thus, in (In,Ga)(As,N)/GaAs QWs, the density of localized states is expected to be much larger than in GaAs/(Al,Ga)As QWs. We have used a spatially resolved CL technique to measure the diffusion length as a function of the detection energy and sample temperature. Both the detection energy and temperature dependence of the diffusion length in the two systems under study are found to be distinctly different, indicating different transport mechanisms in these systems. In order to obtain a better understanding of the diffusion process in (In,Ga)(As,N)/GaAs QWs, we have developed a simple theoretical model, which can explain the experimental results of the detection energy as well as temperature dependence of the diffusion length very well.

II. EXPERIMENT

A GaAs/(Al,Ga)As single QW and three (In,Ga)(As,N)/GaAs single QWs were grown by molecular-beam epitaxy (MBE). A radio-frequency plasma source was used for

TABLE I. Layer parameters, material, and full width at half maximum (FWHM) of the CL spectra of the sample Nos. 1–4. d_w and d_b denote the thickness of the well and top barrier layer.

No.	Well	Barrier	d_w (nm)	d_b (nm)	Substrate	FWHM (meV)
1	GaAs	SPSL	5	175	GaAs(001)	6
2	$\text{In}_{0.24}\text{Ga}_{0.76}\text{As}_{0.98}\text{N}_{0.02}$	GaAs	8	190	GaAs(111)B	50
3	$\text{In}_{0.24}\text{Ga}_{0.76}\text{As}_{0.98}\text{N}_{0.02}$	GaAs	7	250	GaAs(001)	40
4	$\text{In}_{0.3}\text{Ga}_{0.7}\text{As}_{0.98}\text{N}_{0.02}$	GaAs	8	100	GaAs(001)	20

nitrogen during growth of the (In,Ga)(As,N) layers. The growth and the structural properties of these layers have been discussed in detail in Refs. 7 and 8. The layer structures of these samples are described below.

Sample No. 1 was grown on a semi-insulating GaAs(001) substrate containing a 5-nm-thick GaAs well sandwiched between barriers of GaAs (2.4 nm)/AlAs (1.1 nm) short-period superlattices (SPSL). A second GaAs/(Al,Ga)As sample has been fabricated under comparable conditions containing three QWs with varying well width. The QWs were grown on a semi-insulating GaAs(001) substrate. From the bottom to the top, 20-, 15-, and 10-nm-thick well layers have been grown each sandwiched between 30-nm-thick $\text{Al}_{0.3}\text{Ga}_{0.7}\text{As}$ barriers. Sample No. 2 was grown on an *n*-type GaAs(111)B substrate with a miscut angle of 2 deg. The sample consists of an 8-nm-thick (In,Ga)(As,N) well grown between 190 nm GaAs barriers. The whole structure is then sandwiched between a 220-nm-thick beryllium-doped GaAs top layer and an equally thick, silicon-doped GaAs bottom layer. A distinct step-flow growth mode was recognized by reflection high-energy electron diffraction (RHEED) during growth. Sample No. 3 was grown on an *n*-type GaAs(001) substrate and consists of a 7-nm-thick (In,Ga)(As,N) well grown between 250 nm GaAs barriers. The whole structure is then sandwiched between a 300-nm-thick beryllium-doped GaAs top layer and an equally thick, silicon-doped GaAs bottom layer. Note that the RHEED pattern was spotty during growth of the well layer indicating a three-dimensional (3D) growth mode. Sample No. 4, which was grown on a semi-insulating GaAs(001) substrate, consists of an 8-nm-thick (In,Ga)(As,N) well layer grown between a 500 nm bottom and a 100 nm top barrier layer of GaAs. During the growth of the well layer, a magnetic field was applied across the nitrogen plasma beam in order to minimize the ion damage of the layer. Note that sample Nos. 2 and 3 were grown without magnetic field and are thus expected to have a higher defect density than sample No. 4. The parameters describing the structure of these samples are listed in Table I. The FWHM of the CL spectrum, which gives a rough estimate of the degree of disorder, is also listed in Table I.

The diffusion length of the carriers was measured by the method of cathodoluminescence scanning, which was proposed, e.g., by Zarem *et al.*³ The technique is schematically represented in Fig. 1. The carriers are excited by the electron beam of a SEM through a metal mask, which is opaque for the resulting luminescence. The CL signal can be detected, if the excited carriers are able to diffuse from the excitation position to the edge of the mask before recombination takes

place. The metal mask, which consists of a 70-nm-thick Ti and 20-nm-thick Au layer, was fabricated using photolithography and a lift-off technique. As indicated in Fig. 1, the CL intensity (I_{CL}) decreases exponentially as the distance between the excitation position and the edge of the mask (x) is increased. The diffusion length L_d is thus obtained by measuring the absolute value of the inverse slope of $\ln(I_{CL})$ vs x curves. Thus, the technique also allows for a measurement of L_d as a function of the detection energy E . A beam energy of 10 keV was used for all the experiments in this study. This energy value is found to be a reasonable compromise between a good spatial resolution and a sufficient excitation density in the QWs. The spatial resolution of this technique is limited by the abruptness of the mask edges and by the scattering of the incident electrons. In this study, the resolution is estimated to be about 0.2 μm . The measurements were done at various temperatures (T) between 5 and 100 K. The temperature was controlled using a He cooling stage. Sample No. 1 was additionally characterized by spatially resolved photoluminescence (micro-PL) and photoluminescence excitation (PLE) spectroscopy. The probe areas were estimated to be 0.01 mm^2 and 1–2 μm^2 for PLE and micro-PL, respectively.

III. RESULTS AND DISCUSSION

A. Temperature dependence of the diffusion length

Figure 2(a) shows a CL image taken at 65 K of sample No. 1. The CL signal is excited locally with a high spatial resolution all over the shown region of the sample. The emitted CL intensity, however, is collected by a parabolic mirror covering the whole sample surface, i.e., the detection occurs spatially integrated. Therefore, the highest CL intensity is

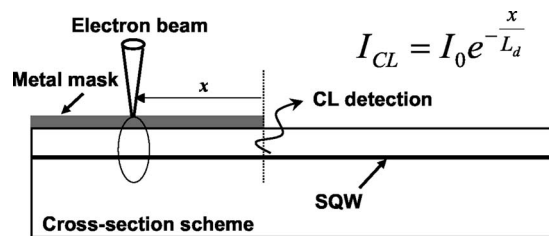


FIG. 1. Schematic diagram of the measurement of the diffusion length L_d of excess carriers for a single quantum well (SQW) by cathodoluminescence in a scanning electron microscope. I_{CL} represents the CL intensity measured as a function of the distance between the excitation spot and the edge of the metal mask x .

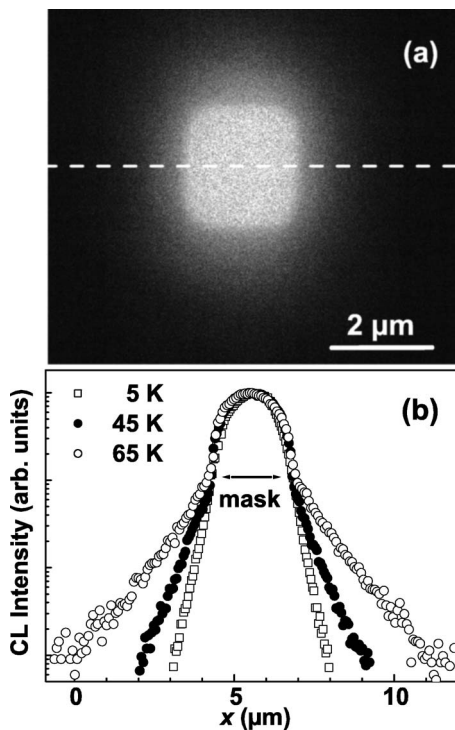


FIG. 2. (a) CL image of sample No. 1 at 65 K. The central bright window represents the mask opening. The halo surrounding the opening manifests the diffusion of excess carriers. (b) CL intensity (logarithmic scale) as a function of the excitation position along a line crossing the mask opening as indicated by the dashed line in (a). For the line scans, the CL detection energy corresponds to the peak energy of the respective CL spectra. For 5, 45, and 65 K, the slope of the exponential decay of the CL intensity corresponds to values of the diffusion length of 0.25, 0.5, and 1 μm , respectively.

detected by a direct excitation of the mask opening. Thus, in the center of the CL image of Fig. 2(a), the mask opening can be seen as a bright zone. If carriers, which are excited at a position outside of the opening namely through the metal mask, can reach the opening by diffusion before radiative recombination takes place, a CL signal is measured, which is assigned to the position of the excitation. Thus, a halo appears near the edges of the mask opening, which can clearly be seen in the image of Fig. 2(a). Note that the metal mask is opaque to the CL. The appearance of the halo directly reflects the carrier diffusion from those regions to the mask opening. In Fig. 2(b), the CL intensity obtained at different temperatures is plotted as a function of the distance between the beam position and the inner edge of the mask. The data are taken along the path indicated by the dashed line in Fig. 2(a). Clearly, in the area under the halo, I_{CL} decays exponentially with x . The absolute value of the slope of the curve decreases as the temperature is increased indicating an increase of L_d with temperature in sample No. 1.

Figure 3 compares the temperature dependence of the diffusion length in sample Nos. 1 (circles) and 4 (triangles). The full and the open symbols represent the data obtained for a detection energy in the low-energy tail and at the peak position of the spectrum, respectively. Clearly, the two samples differ completely in the temperature variation of L_d . While

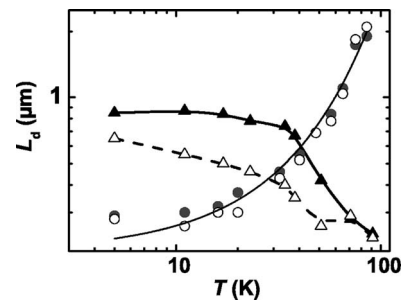


FIG. 3. L_d of sample Nos. 1 (circles) and 4 (triangles) as a function of temperature. Open and solid symbols correspond to a detection energy at the maximum and low-energy region of the CL spectrum, respectively. The lines serve as a guide to the eyes. The difference of the detection energy amounts to about 5 and 20 meV during the measurement of $L_d(T)$ of sample Nos. 1 and 4, respectively.

for sample No. 1 the diffusion length is small at low temperatures but increases as the temperature is increased, which is consistent with the observations of Fig. 2(b), L_d remains essentially unchanged for sample No. 4 as the temperature is increased up to 40 K and then decreases sharply as T is increased further. The two samples also differ in the detection-energy dependence of L_d . While for sample No. 4, the diffusion length measured at the peak position of the spectrum is smaller than the one measured at an energy corresponding to the low-energy tail of the spectrum, there is practically no difference in the values of L_d measured at different detection energies for sample No. 1.

B. Diffusion length as a function of CL detection energy

Figures 4(a) and 4(b) show the detection-energy dependence of L_d measured at 5 K for sample Nos. 1 and 4, respectively. The open symbols in this figure represent the CL spectra. In case of sample No. 1, the diffusion length does not change as the detection energy is scanned over the spectrum, which is in accordance with the results for this sample shown in Fig. 3. In fact, the diffusion length is found to be energy independent at all temperatures up to 100 K in this sample. However, the diffusion length clearly decreases as E is scanned from the low- to the high- E side of the spectrum in sample No. 4. This observation is consistent with the results shown in Fig. 3 for this sample.

In Figs. 5(a) and 5(b), the diffusion length measured at 5 K is plotted as a function of E for the (In,Ga)(As,N)/GaAs sample Nos. 3 and 2, respectively. The CL spectra of these samples are also shown (open symbols) in the respective panels. Unlike in the GaAs/(Al,Ga)As QW (sample No. 1), the diffusion length in all of these (In,Ga)(As,N)/GaAs QWs clearly decreases as the detection energy increases. However, the dependence of L_d on E varies from sample to sample. The dependence is clearly strongest in sample No. 4 [cf. Fig. 4(b)] and weakest in sample No. 2 [cf. Fig. 5(b)]. Note that sample No. 2 is showing the broadest CL spectrum among all (In,Ga)(As,N)/GaAs QWs, while in sample No. 4 the spectrum is clearly the narrowest. In fact, the quantum efficiency

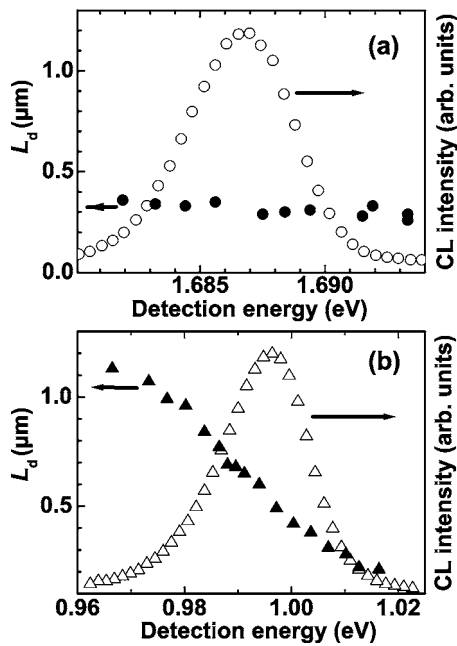


FIG. 4. L_d (solid symbols) of (a) sample Nos. 1 and (b) 4 as a function of the CL detection energy at 5 K. The open symbols represent the respective CL spectra.

(the CL intensity) is also found to be the highest in sample No. 4 and the lowest in sample No. 2 among all the dilute nitride QWs.

C. Disorder and its influence on the carrier transport

Figure 6(a) shows the micro-PL and absorption spectra for sample No. 1. The latter has been semi-empirically derived

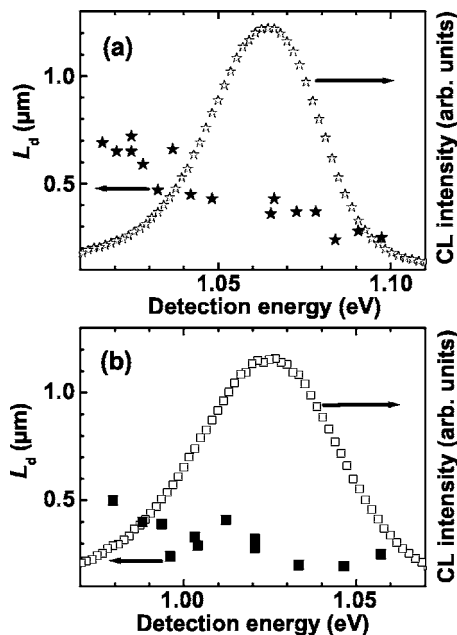


FIG. 5. L_d (solid symbols) of (a) sample Nos. 3 and (b) 2 as a function of the CL detection energy at 5 K. The open symbols represent the respective CL spectra.

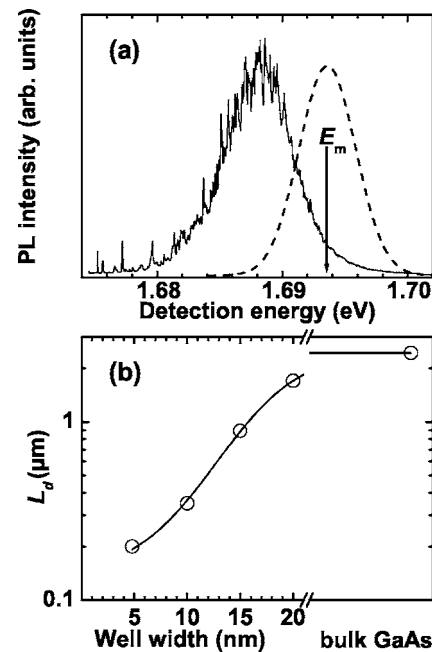


FIG. 6. (a) Micro-PL (solid line) and absorption (dashed line) spectrum of sample No. 1 at 5 K. The absorption spectrum has been derived from the PL excitation spectrum. E_m denotes the effective mobility edge of excited carriers in the QW. (b) L_d of GaAs/(Al,Ga)As QWs as a function of well width at 5 K. The 5-nm-thick QW is identical with sample No. 1, the 10-, 15-, and 20-nm-thick QWs belong to the multiple QW sample as described in Sec. II. The line serves as a guide to the eyes.

from the respective PLE spectrum as described in Ref. 9. Clearly, there is an energy difference between the peak positions of the two spectra. The difference in energy (Stokes shift) is found to be about 5 meV. It is also clear from Fig. 6 that the micro-PL spectrum consists of a large number of spikes distributed over the whole spectrum. These narrow spikes are associated with the radiative recombination of localized excitons.^{9,10} Previously, we have studied the variation of the energy distribution of these narrow spikes as a function of the excitation energy in similar samples to determine the energy boundary between the localized and the extended states, the so-called effective mobility edge E_m .⁹ As expected, E_m is found to be at the peak position of the absorption spectrum. Thus, almost the entire PL spectrum lies below the mobility edge, which indicates that mostly localized states are responsible for the photoluminescence signal. In this case, interface roughness is probably the main cause for the carrier localization.¹¹ Figure 6(b) shows L_d as a function of the well width of GaAs/(Al,Ga)As single QWs measured at 5 K. L_d clearly increases as the thickness of the QW is increased, demonstrating the impact of interface roughness on carrier transport. Since interface roughness is well controlled during growth, a low density of localized states is expected to exist in GaAs/(Al,Ga)As QWs. We have estimated from the number of spikes in the micro-PL spectrum a localized state density of 10^9 – 10^{10} cm⁻² in sample No. 1.

Figure 7(a) shows the CL spectra taken at an electron-beam current (i_b) of 0.12 (circles) and 15 nA (squares) for sample No. 4. Clearly, there is a blueshift as well as a broad-

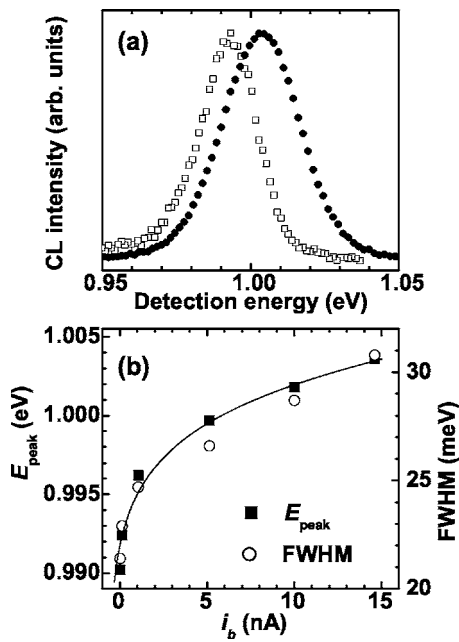


FIG. 7. (a) CL spectra of sample No. 4 for an electron beam current of 0.12 (circles) and 15 nA (squares) at 5 K. (b) Peak energy (squares) and FWHM (circles) of the CL spectra of sample No. 4 as a function of the electron beam current (i_b) at 5 K. The solid line serves as a guide to the eyes.

ening of the spectrum as the excitation density is increased, which indicates a band filling effect. In Fig. 7(b), the peak energy (E_{peak}) and the FWHM of the CL spectrum is plotted as a function of i_b . Note that both the peak energy and the FWHM exhibit the same functional dependence on i_b . In fact, these features are found in all (In,Ga)(As,N)/GaAs QW samples suggesting the existence of a large density of localized states in (In,Ga)(As,N)/GaAs QWs. Interface roughness is surely not the main cause for the localization in this case, since a qualitatively similar blueshift as well as a broadening of the spectrum with increasing excitation density have been observed even in bulk (In,Ga)(As,N) layers,¹² where interface effects can be excluded. In (In,Ga)(As,N) QWs, the main cause of localization would thus be alloy inhomogeneities. The repulsion between N-Ga_mIn_{4-m} cluster states and the states in the conduction band minimum results in fluctuations of the band structure. Since the energy and the density of such states depend strongly on m and on the concentration of N, a broad distribution of band tail states is expected in this case.²

The local minima (maxima) of the potential fluctuations can trap electrons (holes), leading to the formation of localized states below the conduction band edge (CBE) [above the valence band edge (VBE)]. Depending on the length scale of the fluctuations, two situations can readily be distinguished as depicted schematically in Fig. 8. In case (i), the average spatial separation between the minima is so large that tunneling between localized states is suppressed. An opposite situation can be imagined, when the length scale of the fluctuations is so small that tunneling between states is allowed [case (ii) in Fig. 8]. This leads to the formation of a fluctuation band as shown in Fig. 9. A third situation can

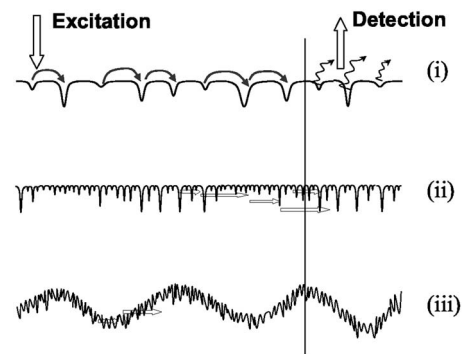


FIG. 8. Schematic diagram of several possible potential variations acting as localization centers in QWs. (i) Low density of localization centers caused, e.g., by interface roughness. For low T , transport is possible only by hopping. (ii) Short-range variations caused, e.g., by alloy fluctuations. Transport is possible by tunneling between the localization centers. (iii) Superposition of long-range and short-range fluctuations. Tunneling is suppressed by the long-range disorder.

arise when short-range fluctuations are superimposed by band structure modulations on a much larger length scale as schematically depicted in case (iii) of Fig. 8.

After generation, the electron-hole pairs are rapidly captured in the local minima. Given that the density of the excitation is less than the density of localized states, all excited carriers would immediately be trapped in the minima. The temperature and detection-energy dependence of the diffusion length in the three considered cases exhibit a distinctly different behavior as described below.

In case (i), there are only two paths available for carrier diffusion. The first one is thermal hopping between localized states and the second one is thermal activation into the band of delocalized states. There will be no diffusion at low temperatures, since both channels are practically ineffective. At sufficiently high temperatures, the diffusion is most effectively driven by delocalized band states, since the mobility through these states is expected to be much larger than the hopping conduction through the localized states. The diffusion length is thus expected to increase with increasing

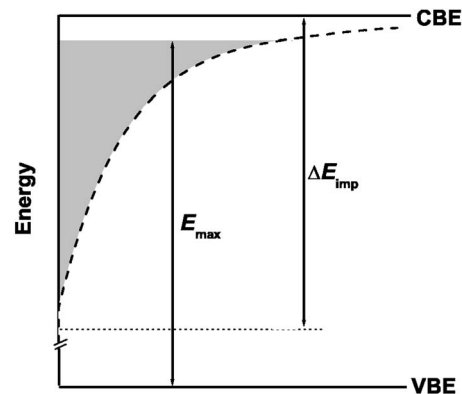


FIG. 9. Schematic diagram of the energy distribution of localized states for case (ii) of Fig. 8. E_{max} is the energy, up to which all levels of the fluctuation band are filled for a certain generation rate G . ΔE_{imp} denotes the width of the fluctuation band.

temperature.⁵ Note that a qualitatively similar behavior is observed in sample No. 1 as shown in Fig. 3. Moreover, the diffusion length, which can be expressed as $L_d = \sqrt{D\tau}$, where D denotes the diffusion coefficient and τ the carrier recombination time for the band states, is clearly independent of the initial/final energy state of the carrier before/after the diffusion. L_d is thus expected to be independent of the detection energy, which is consistent with the results shown in Figs. 3 and 4(a) for sample No. 1.

In case (ii), the excited carriers can diffuse through the fluctuation band leading to a very different temperature and detection-energy dependence of L_d . Since in this case, the transport is tunneling assisted, a very weak temperature dependence of L_d is expected. This is consistent with the results of Fig. 3 for sample No. 4 at least up to 40 K. Note that the sudden decrease of L_d above 40 K observed in this sample can be attributed to a thermal activation of nonradiative recombination channels, which is probably due to the high density of point defects usually observed in dilute nitride layers.¹³ While diffusing through the fluctuation band, the carriers with energy E can be captured by states below E . The higher the value of E , the larger will be the number of states involved in this capture process. This intraband capture, which is expected to be a much faster process than the electron-hole recombination, determines the diffusion length. The diffusion length is thus expected to decrease as the detection energy is increased. This is consistent with the results of Figs. 3 and 4(b) for sample No. 4. The density of band structure fluctuations in sample No. 4 is estimated to be so large that the situation can be identified as case (ii).

In case (iii), diffusion takes place in a fluctuation band, which is additionally modulated due to long-range disorder. If the amplitude of the modulation is sufficiently large, the carriers can diffuse only by thermal activation. The situation will be very similar to case (i). However, when the amplitude of the modulation is not large enough so that the carriers can diffuse through the band without thermal activation, the diffusion length is expected to show a qualitatively similar, but much weaker energy dependence than in case (ii). Note that the energy dependence of L_d in sample Nos. 3 and 2 exhibits a qualitatively similar behavior as the one observed in sample No. 4. However, the detection-energy dependence of L_d in these sample [No. 3: Fig. 5(a), and No. 2: Fig. 5(b)] is much weaker than the one in sample No. 4 [Fig. 4(b)], which suggests that sample Nos. 3 and No. 2 belong to case (iii). As mentioned above, the RHEED pattern has demonstrated a step-flow growth mode for sample No. 2. In fact, SEM images of this sample (not shown) reveal a large number of triangular-shaped structures on the surface, which are believed to be formed due to step bunching during growth. Moreover, the RHEED pattern of sample No. 3 indicates a 3D growth. Both the surface morphology of sample No. 2 and the RHEED pattern of sample No. 3 indicate the occurrence of a long-range roughness and thus a large-scale lateral modulation of the band gap in these samples.

D. Model

We have developed a simple model to obtain a better understanding for case (ii). We consider that all the generated

electron-hole pairs eventually form free excitons and are finally trapped in the fluctuation band which in fact is the case at least at low temperatures. The diffusion length of excitons with an energy E in the fluctuation band can be expressed as

$$L_d(E) = \sqrt{D_f(E)\tau_f(E)}, \quad (1)$$

where $D_f(E)$ is the diffusion coefficient associated with energy E and $\tau_f(E)$ the average time an exciton spends in the energy level E before being captured by states below E . $\tau_f(E)$ is determined by the combined capture rate of the states below E and is expected to be much smaller than the recombination lifetime of the excitons. The capture rate for an individual level $1/\tau_c(E) = v_{th}\sigma N_f(E)$, where $v_{th} = \sqrt{3k_B T/m^*}$ is the average thermal velocity of the excitons at temperature T , m^* is the excitonic effective mass, k_B is the Boltzmann constant, σ is the capture cross section, which is assumed to be the same for every energy state of the band, and $N_f(E)$ is the density of states of the band. Since it is intuitively expected that the deeper the fluctuation the lower will be the density of the corresponding localized states, $N_f(E)$ should decrease as the distance of E from the conduction band minimum is increased. Here, we assume $N_f(E) = N_0 e^{-\alpha E}$, where N_0 and α are energy-independent constants.

Now, $\tau_f(E)$ will be given by

$$\frac{1}{\tau_f(E)} = \int_E^\infty \frac{1}{\tau_c(E)} dE = \frac{\sigma v_{th} N_0}{\alpha} \exp(-\alpha E), \quad (2)$$

and the diffusion length becomes

$$L_d(E) = \sqrt{\frac{D_f(E)\alpha}{\sigma v_{th} N_0}} \exp\left[\frac{\alpha E}{2}\right]. \quad (3)$$

The diffusion coefficient $D_f(E)$, which is expected to be determined by the tunneling probability between the minima, can be expressed as $D_f(E) = D_0 e^{-\gamma d(E)}$, where $d(E) = (N_0 e^{-\alpha E})^{-1/3}$ is the average separation between the minima associated with energy E . D_0 and γ are energy-independent constants.

Finally, we make a transformation $E \rightarrow [E_g - E]$ to change the energy reference from the conduction band minimum to the valence band maximum. Equation (3) can now be rewritten as

$$\ln[L_d(E)] = \ln A - \frac{\alpha}{2} E - \frac{B}{2} \exp\left[-\frac{\alpha E}{3}\right], \quad (4)$$

where $A = \sqrt{D_0 \alpha e^{\alpha E_g} / \sigma v_{th} N_0}$ and $B = \gamma N_0^{-1/3} e^{(\alpha E_g/3)}$ are energy-independent constants.

We have used Eq. (4) to fit the experimental dependence of L_d on the detection energy for sample No. 4 with A , B , and α as fit parameters. The experimental data as well as the best fit of our model to the data are shown in Fig. 10(a). The fits reproduce the general trend very well and return the following values for the parameters: $\ln A = 58.8$, $B = 1.0 \times 10^{17}$, and $\alpha = 118.5 \text{ eV}^{-1}$. Except for α , the rest of the unknown parameters cannot be obtained independently from this fit, since the total number of the unknown parameters (D_0 , N_0 , σ , γ ,

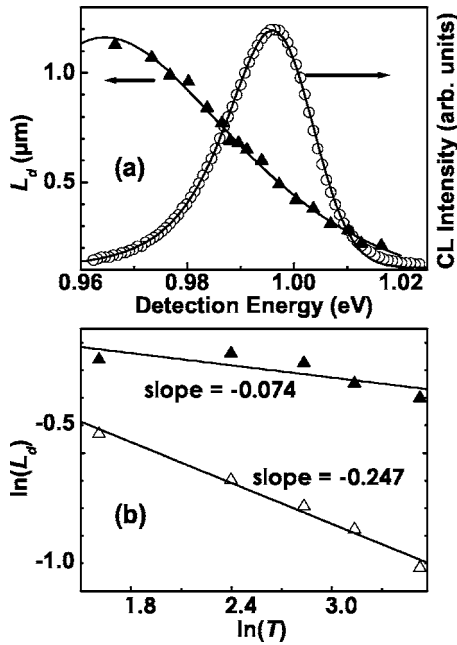


FIG. 10. (a) L_d of sample No. 4 as a function of the CL detection energy at 5 K. (b) $\ln(L_d)$ of sample No. 4 as a function of $\ln(T)$, where the filled and open symbols represent data points obtained for E values set to the low- E range and peak energy of the CL spectrum, respectively. In (a) and (b), the solid lines represent the results of the model calculation.

and α) is larger than the number of fit parameters. The width of the fluctuation band ($\Delta E_{\text{imp}} = 1/\alpha$) can be estimated to be about 8 meV.

According to this model, the temperature dependence of the diffusion length should arise only through v_{th} . From Eq. (4), $L_d(T)$ can be expressed as

$$L_d(T) = CT^{-1/4}, \quad (5)$$

where $C = \sqrt{D_0 \alpha \sqrt{m^*} e^{-\gamma d(E)} e^{\alpha(E_g - E)} / \sigma \sqrt{3k_B N_0}}$ is a temperature-independent constant. Thus, the diffusion length for the (In,Ga)(As,N)/GaAs QWs is expected to follow a very weak temperature dependence, which is consistent with the observations in Fig. 3 for sample No. 4. The open triangles in Fig. 10(b) represent the double logarithmic plot of the temperature dependence (up to 35 K) of the diffusion length obtained at the peak energy of the CL spectrum for sample No. 4. The plot clearly demonstrates a linear behavior with a slope of $-1/4$, which corresponds to the power law of Eq. (5) proving the consistency of our model. Note that the diffusion process associated with energy levels deep in the tail of the density of states is unlikely to be strictly tunneling-assisted, since the average separation between the minima [$d(E)$] increases exponentially with the decrease of the density of states. For those energy levels, the hopping conduction of the carriers should also play a significant role in the diffusion process. However, this effect is not taken into account in this simple model. Since the hopping conduction increases with temperature, the diffusion length is intuitively

expected to follow a temperature dependence, which is even weaker than $T^{-1/4}$. The filled triangles of Fig. 10(b) represent the double logarithmic plot of the temperature dependence (up to 35 K) of L_d measured at a detection energy in the tail of the CL spectrum of sample No. 4, which indeed displays a much weaker temperature dependence than $T^{-1/4}$.

Another estimate of α can be made from the line shape of the CL spectrum, which should also carry the signature of the density-of-state distribution. Let us assume that at a certain generation rate G , all the levels up to $E = E_{\text{max}}$ of the fluctuation band are filled by the excitons as shown schematically in Fig. 9. We further assume that the rate of the radiative recombination from each level is only determined by the density of states associated with that level. The effective line shape can be expressed as

$$I_{\text{eff}} = \int_{E_{\text{max}}}^{\infty} I_0 \exp\left[-\frac{(E - E_0)^2}{2\sigma_0^2}\right] N_0 \exp(-\alpha E_0) dE_0. \quad (6)$$

Here, we associate a Gaussian line shape $I_0 \exp[-(E - E_0)^2/2\sigma_0^2]$ with every level of the distribution. We use Eq. (6) to fit the experimental line shape of the CL spectrum of sample No. 4 with E_{max} , α , and σ_0 as fit parameters. Figure 10(a) shows the experimental spectrum as well as the best fit to the data. The best fit is obtained with $E_{\text{max}} = 0.998$ eV, $\sigma_0 = 8.5$ meV, and $\alpha = 121$ eV $^{-1}$. Note that a very similar value of α was obtained earlier from the fit to the dependence of L_d on E within our model.

IV. CONCLUSIONS

Both the temperature and CL detection-energy dependence of the diffusion length in (In,Ga)(As,N)/GaAs QWs are found to be extremely different from the ones in GaAs/(Al,Ga)As QWs. While in GaAs/(Al,Ga)As QWs the diffusion length as a function of the detection energy is found to be practically unchanged, in dilute nitride QWs L_d decreases with increasing detection energy. However, L_d is found to be an increasing function of T in GaAs/(Al,Ga)As QWs, while in dilute nitride QWs L_d shows a temperature-independent behavior. This distinctly different temperature and detection-energy dependence of L_d in the two investigated material systems is attributed to the difference in the transport mechanism of the carriers. The experimental results can be understood in terms of a thermally activated carrier transport mechanism in GaAs/(Al,Ga)As QWs and a tunneling-assisted transport of the carriers in dilute nitride QWs. The measurement of the energy-resolved diffusion length using the CL scanning technique can thus be a powerful technique to distinguish between hopping- and tunneling-assisted carrier transport mechanisms in semiconductor structures.

ACKNOWLEDGMENTS

We would like to thank H. T. Grahn for comments and for a critical reading of the manuscript as well as E. Wiebicke and A. K. Bluhm for the assistance in the sample processing.

*Electronic address: ujahn@pdi-berlin.de

- ¹P. R. C. Kent and A. Zunger, *Phys. Rev. Lett.* **86**, 2613 (2001).
- ²K. Kim and A. Zunger, *Phys. Rev. Lett.* **86**, 2609 (2001).
- ³H. A. Zarem, P. C. Sercel, J. A. Lebens, L. E. Eng, A. Yariv, and K. J. Vahala, *Appl. Phys. Lett.* **55**, 1647 (1989).
- ⁴L. L. Chao, G. S. Cargill, E. Snoeks, T. Marshall, J. Petruzzello, and M. Pashley, *Appl. Phys. Lett.* **74**, 741 (1999).
- ⁵H. Hillmer, A. Forchel, S. Hansmann, M. Morohashi, E. Lopez, H. P. Meier, and K. Ploog, *Phys. Rev. B* **39**, 10901 (1989).
- ⁶J. Hegarty, L. Goldner, and M. D. Sturge, *Phys. Rev. B* **30**, R7346 (1984).
- ⁷J. Miguel-Sánchez, A. Guzmán, J. M. Ulloa, A. Hierro, and E. Muñoz, *Appl. Phys. Lett.* **84**, 2524 (2004).
- ⁸J. Miguel-Sánchez, A. Guzmán, and E. Muñoz, *Appl. Phys. Lett.* **85**, 1940 (2004).
- ⁹U. Jahn, M. Ramsteiner, R. Hey, H. T. Grahn, E. Runge, and R. Zimmermann, *Phys. Rev. B* **56**, R4387 (1997).
- ¹⁰U. Jahn, S. H. Kwok, M. Ramsteiner, R. Hey, H. T. Grahn, and E. Runge, *Phys. Rev. B* **54**, 2733 (1996).
- ¹¹D. Gammon, B. V. Shanabrook, and D. S. Katzer, *Phys. Rev. Lett.* **67**, 1547 (1991).
- ¹²R. A. Mair, J. Y. Lin, H. X. Jiang, E. D. Jones, A. A. Allermann, and S. R. Kurtz, *Appl. Phys. Lett.* **76**, 188 (2000).
- ¹³C. H. Fischer and P. Bhattacharya, *J. Appl. Phys.* **96**, 4176 (2004).